

## **General Disclaimer**

### **One or more of the Following Statements may affect this Document**

- This document has been reproduced from the best copy furnished by the organizational source. It is being released in the interest of making available as much information as possible.
- This document may contain data, which exceeds the sheet parameters. It was furnished in this condition by the organizational source and is the best copy available.
- This document may contain tone-on-tone or color graphs, charts and/or pictures, which have been reproduced in black and white.
- This document is paginated as submitted by the original source.
- Portions of this document are not fully legible due to the historical nature of some of the material. However, it is the best reproduction available from the original submission.

(NASA-CR-120521) EXPERIMENTAL  
INVESTIGATION OF ELECTRON CLOUD  
CONTAINMENT IN A NONUNIFORM MAGNETIC  
FIELD (Avco-Everett Research Lab.) 43 p  
HC \$3.75

N75-11152

CSCL 09C G3/33 Uncl:s  
02363

EXPERIMENTAL INVESTIGATION  
OF ELECTRON CLOUD CONTAINMENT  
IN A NONUNIFORM MAGNETIC FIELD

J. E. Eninger

RESEARCH REPORT 400

Contract No. NAS8-24140

May 1974

supported by

GEORGE C. MARSHALL SPACE FLIGHT CENTER  
National Aeronautics and Space Administration  
Marshall Space Flight Center, Alabama 35812

 **AVCO** EVERETT RESEARCH LABORATORY, INC.

A SUBSIDIARY OF AVCO CORPORATION



RESEARCH REPORT 400

EXPERIMENTAL INVESTIGATION OF ELECTRON CLOUD  
CONTAINMENT IN A NONUNIFORM MAGNETIC FIELD

by

J. E. Eninger

AVCO EVERETT RESEARCH LABORATORY, INC.  
a Subsidiary of Avco Corporation  
Everett, Massachusetts 02149

Contract No. NAS8-24140

May 1974

supported by

GEORGE C. MARSHALL SPACE FLIGHT CENTER  
NATIONAL AERONAUTICS AND SPACE ADMINISTRATION  
Marshall Space Flight Center, Alabama 35812

## ABSTRACT

Dense clouds of electrons are generated and studied in an axisymmetric, nonuniform magnetic field created by a short solenoid. The operation of the experiment is similar to that of a low-pressure ( $\sim 10^{-6}$  Torr) magnetron discharge. Discharge current characteristics are presented as a function of pressure, magnetic field strength, voltage, and cathode end-plate location. The rotation of the electron cloud is determined from the frequency of diocotron waves. In the space charge saturated regime of operation, the cloud is found to rotate as a solid body with a frequency close to  $V_a/\phi_a$  where  $V_a$  is the anode voltage and  $\phi_a$  is the total magnetic flux. This result indicates that, in regions where electrons are present, the magnetic field lines are electrostatic equipotentials ( $\bar{E} \cdot \bar{B} = 0$ ). Equilibrium electron density distributions suggested by this condition are integrated with respect to total ionizing power and are found consistent with measured discharge currents.

---

PRECEDING PAGE BLANK NOT FILMED

## TABLE OF CONTENTS

<u>Section</u>		<u>Page</u>
	Abstract	vi
	List of Illustrations	vii
I.	INTRODUCTION	1
II.	EXPERIMENTAL APPARATUS	3
III.	THEORY	11
	1. Discharge Characteristics	11
	2. Electron Cloud Equilibria	16
	3. Electron Cloud Stability	18
IV.	EXPERIMENTAL OBSERVATIONS	21
	1. Discharge Current	21
	2. Diocotron Waves	29
V.	DISCUSSION AND CONCLUSIONS	33
VI.	ACKNOWLEDGMENTS	39
VII.	REFERENCES	41

PRECEDING PAGE BLANK NOT FILMED

## LIST OF ILLUSTRATIONS

<u>Figure</u>		<u>Page</u>
1	Schematic Drawing of the Experimental Apparatus	4
2	Electrical Diagram of the Solenoid Experiment	5
3	Magnetic Field Configuration Produced by the Solenoid	6
4	Discharge Current vs Applied Magnetic Field (in the Center of the Coil) with Conducting End-Plates Positioned 1 cm from the Anode ( $z_e = 5.5$ cm)	8
5	Typical Diocotron Wave Traces Shown on a Slow and a Fast Time Scale	9
6	a) Cylindrical Penning Discharge Geometry used as an Idealized Model for Deriving Discharge Characteristics b) Schematic Representation of the Radial Potential Profiles Corresponding to Different Regimes of Operation as Explained in the Text	13
7	Pressure and Voltage Dependence of the Normalized Discharge Current for Space Charge Saturated Conditions	22
8	Discharge Characteristics Obtained for $p = 2 \times 10^{-6}$ Torr with the End-Plates Positioned at $z_e = 5.5$ cm	24
9	Relationship between Anode Voltage $V_a$ and Magnetic Field $B_s$ (in Terms of $I_m$ ) at the Space Charge Saturation Point (3) for the Data shown in Fig. 8	25
10	Discharge Current $I_s$ at the Saturation Point (3) for the Data shown in Fig. 8	26
11	Discharge Characteristics Obtained for $p = 2 \times 10^{-6}$ Torr with End-Plates Positioned Far Apart ( $z_e = 14.5$ cm)	27
12	Saturation Current $I_s$ at as a Function of End-Plate Location for Different Anode Voltages	28
13	The Points show Measured $\ell = 2$ Mode Diocotron Wave Frequencies Plotted vs the Ratio of Anode Voltage to Magnet Current	30

<u>Figure</u>		<u>Page</u>
14	Diocotron Wave Frequency Spectrum Measured with the End Plates Located Far Apart ( $z_e = 12$ cm)	31
15	Computer Solutions of Laplace's Equation for Two Different End-Plate Locations (a) $z_e = 5.4$ cm and (b) $z_e = 9.4$ cm	34
16	Comparison of Measured and Calculated Currents for Different End-Plate Locations	36

## I. INTRODUCTION

The space charge of electrons plays an important role in controlling the behavior of a number of devices working with crossed electric and magnetic fields. The magnetron configuration, for example, can be operated in either an unstable mode for the generation of microwaves, or in a stable mode as a pressure gauge. The difference between the two modes can be characterized by a dimensionless parameter  $q = \omega_p^2 / \omega_c^2$ , where  $\omega_p$  is the electron plasma frequency and  $\omega_c$  is the electron gyro frequency.<sup>1</sup> Thus, while the magnetron tube operates close to  $q = 1$ , stable electron cloud confinement requires  $q \ll 1$ . Stability conditions also depend on the shape of the electron cloud. A thin crossed-field electron beam, for example, can be unstable even for small values of  $q$  due to the diocotron effect.<sup>1-3</sup> Furthermore, an ion-electron resonance instability has been predicted<sup>4</sup> and verified by experiments<sup>5</sup> for electron cloud configurations in which ions are trapped and contained.

Another important consideration is the existence of equilibrium density distributions for magnetically confined electron clouds. Such equilibria have been demonstrated theoretically<sup>6</sup> and experimentally<sup>5</sup> for toroidal magnetic fields. For certain other geometries, such as the low-pressure magnetron and Penning discharges,<sup>7-9</sup> the shape of the electrostatic field prevents the electrons from occupying the full length of the magnetic field lines. In regions where electrons are present, the magnetic field lines must be equipotentials of the electrostatic field ( $\vec{E} \cdot \vec{B} = 0$ ),

whereas Laplace's equation applies in regions that are void of electrons. As has been pointed out by Levy,<sup>10</sup> the problem of calculating the geometrical boundary of the electron cloud in this type of configuration is difficult, particularly when the strength of the magnetic field varies in space.

In this paper, we describe an experiment in which dense clouds of electrons are generated in an axisymmetric magnetic field created by a short solenoid. The operation of the experiment is similar to that of a low-pressure ( $\sim 10^{-6}$  Torr) magnetron discharge. An important feature is that the electron cloud is allowed to occupy regions of high as well as low magnetic field, a situation which enables us to study the equilibrium and stability of electron clouds with substantial gradients in density and in the parameter  $q$ . These conditions are representative of the Plasma Radiation Shield,<sup>11</sup> a crossed-field electron device proposed for protecting manned space-vehicles against proton radiation from solar flares.

Section II of the paper describes the experimental apparatus and diagnostics used for the present studies. In Section III we discuss the theory that is relevant to the experiment. This includes discharge characteristics as well as the equilibrium and stability of magnetically confined electron clouds. The experimental observations are described in Section IV and compared with theoretical predictions in Section V.

## II. EXPERIMENTAL APPARATUS

The apparatus used in the present experiments is shown schematically in Fig. 1, and consists of a solenoid magnet coil (2) enclosed in a stainless steel toroidal shell, which is shaped to match a magnetic flux surface and serves as the anode of the discharge. This structure is supported by two struts (3) and insulated electrically (4) from the  $\approx 10^{-7}$  Torr vacuum chamber (1). Azimuthally symmetric pyrex insulators (6) have been introduced in order to eliminate possible interference of the support struts with the discharge. The combination of a 0.5 mm diameter tungsten filament (7) located along the axis of symmetry, two end plates (5) and two cylindrical shields made of stainless steel constitute the cathode of the discharge cell. The filament can be operated either hot or cold (most of the experiments were done with a cold filament) and the end plates are movable to allow variation of the experimental boundary conditions.

Figure 2 shows a circuit diagram indicating power supplies and instrumentation used for obtaining discharge characteristics. Voltages of up to 10 kV are applied between anode and cathode. The 500 V supply shown is used for backbiasing the hot filament; this is to prevent current from flowing between the filament and the rest of the cathode structure. The air-cooled solenoid magnet is powered by low voltage batteries and produces the d. c. magnetic field configuration shown in Fig. 3. The agreement between this calculated field shape and the measured field is better than 3%. Magnetic fields of up to 1300 G in the center of the coil were used in the experiments.

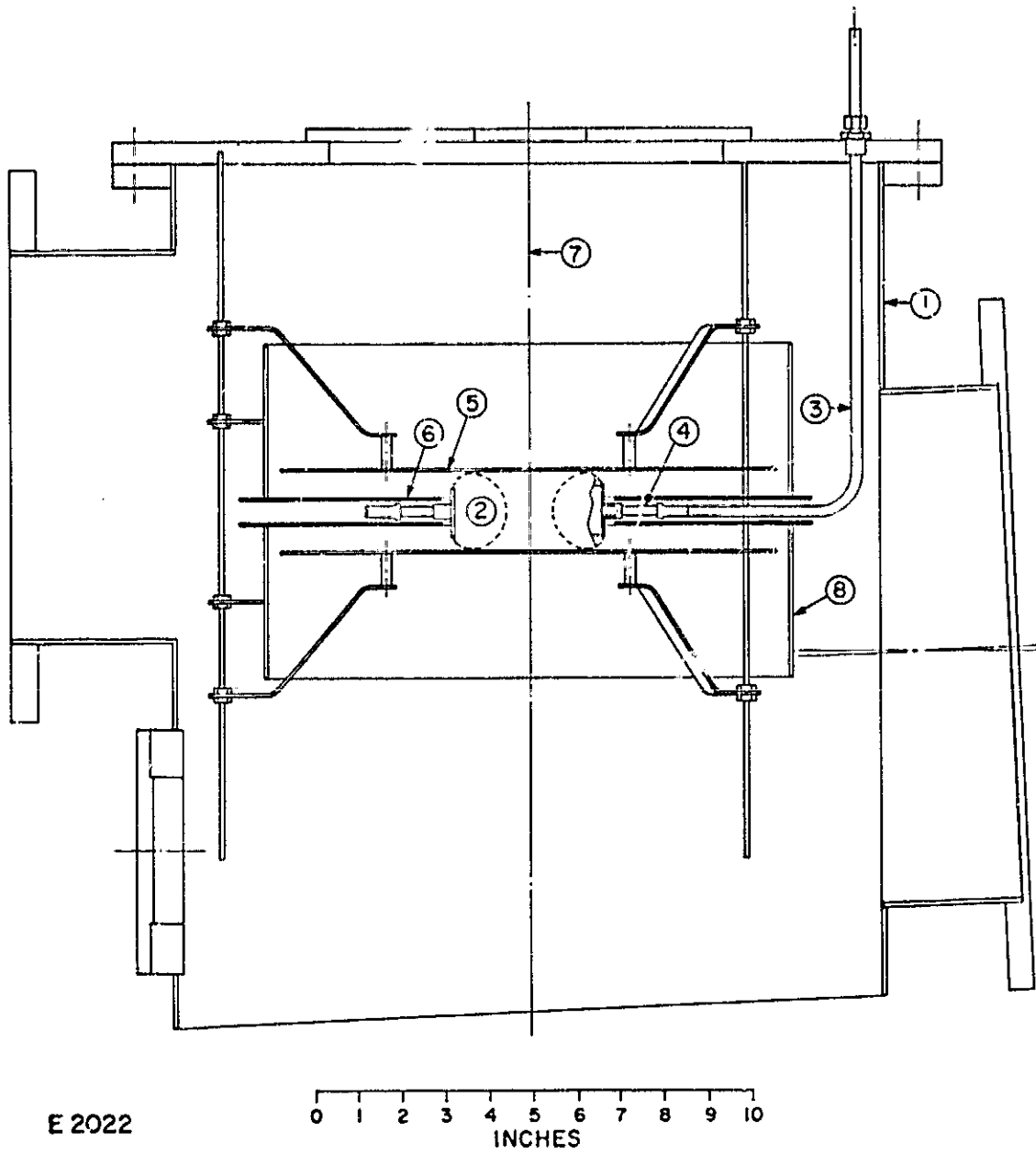
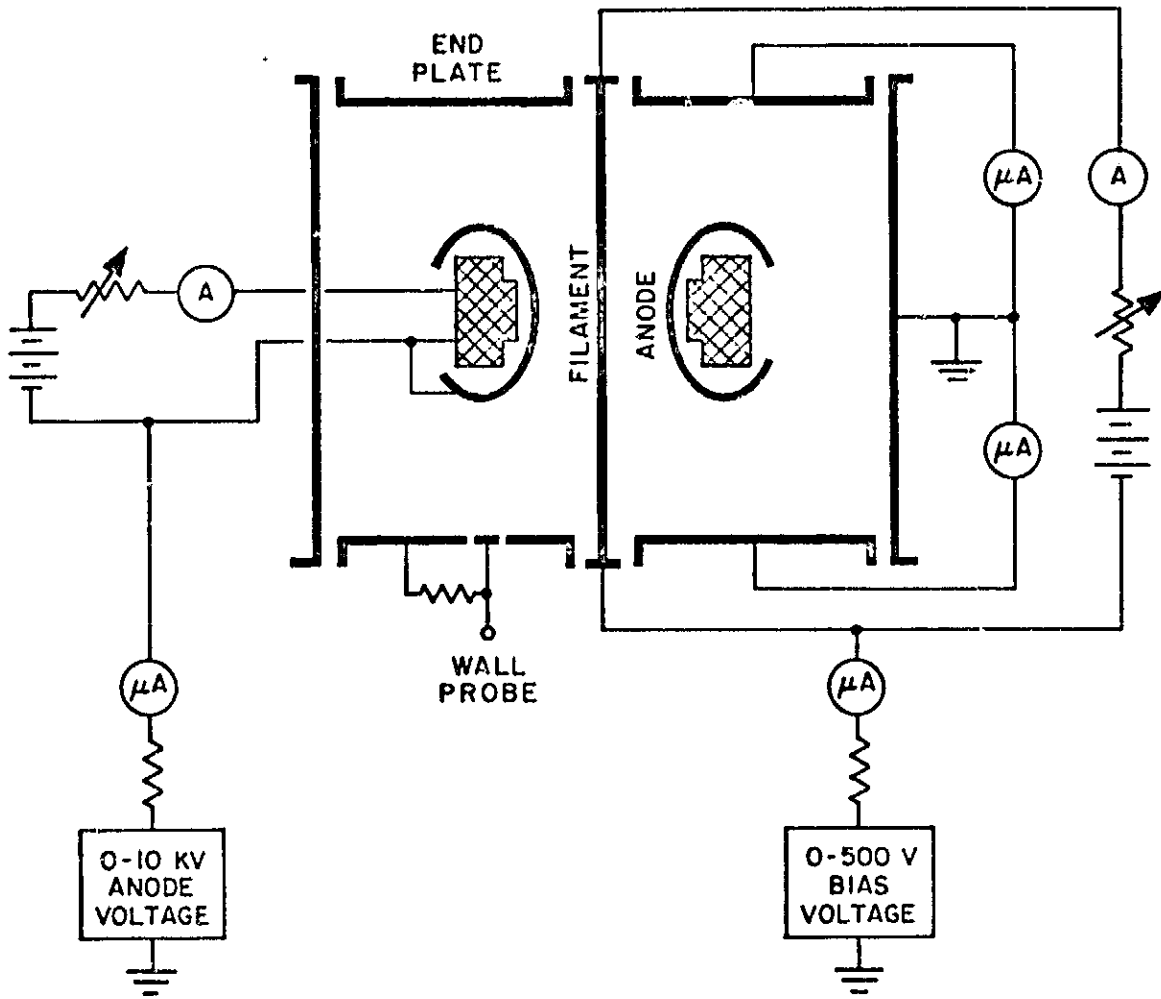
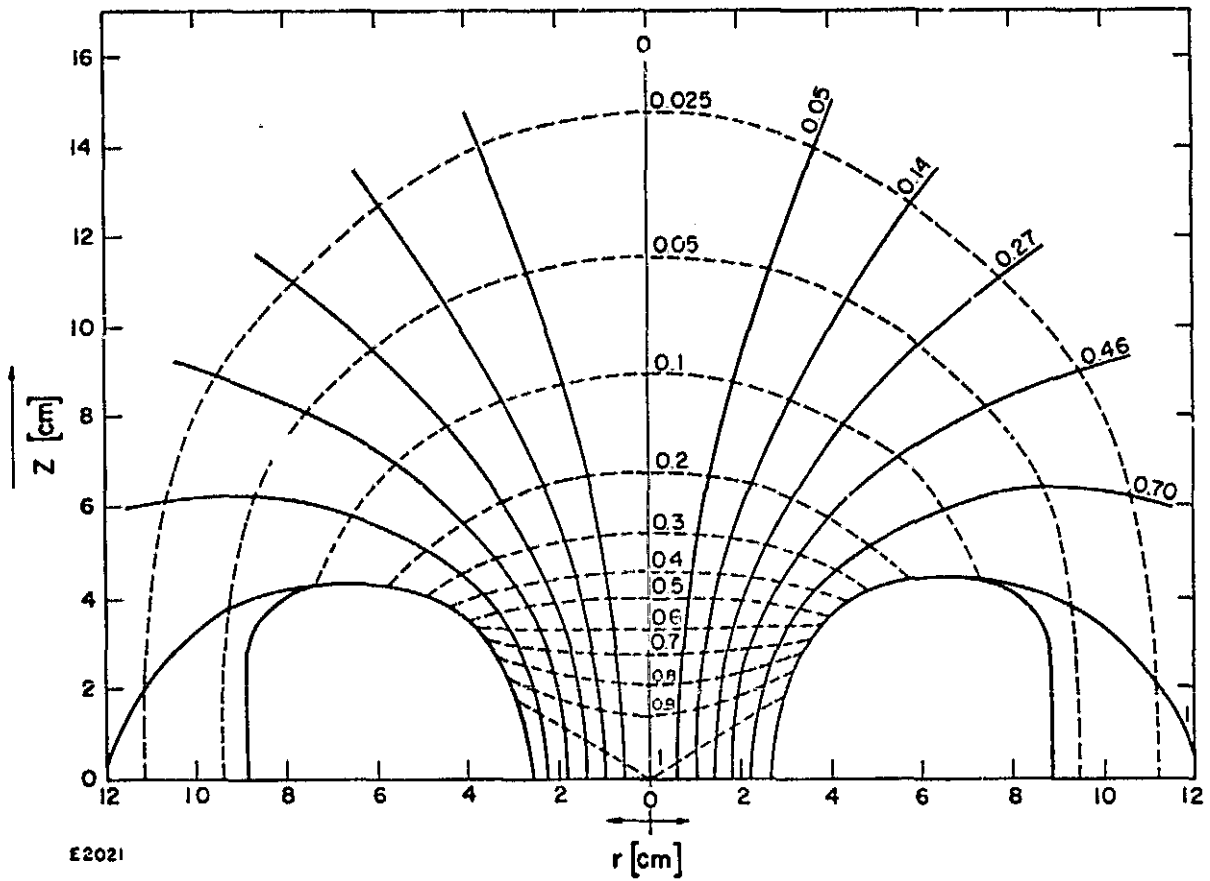


Fig. 1 Schematic drawing of the experimental apparatus. The various components shown are described in the text.



B4657

Fig. 2 Electrical diagram of the solenoid experiment.



£2021

Fig. 3 Magnetic field configuration produced by the solenoid. The solid lines are magnetic field lines with the normalized flux  $\phi$  indicated. The dashed lines represent constant  $B$  normalized to the field in the center of the coil.

Figure 4 shows typical discharge characteristics obtained with the end-plates positioned 1 cm from the anode ( $z_e = 5.5$  cm in Fig. 3) for operation with hot and cold filament, respectively. These curves will be discussed in more detail in Section III.

A diagnostic tool used primarily to study the stability of the electron cloud and to measure its rotational velocity is the so-called "current-button,"<sup>5</sup> which can be described as an electrostatic wall probe with flat frequency response up to about 100 MHz. Several such 1 cm diameter probes were located on the end-plates (see Fig. 2) at different radial as well as azimuthal positions. Figure 5 shows current-button oscilloscope traces due to diocotron waves which are induced on the surface of the electron cloud under certain operating conditions.

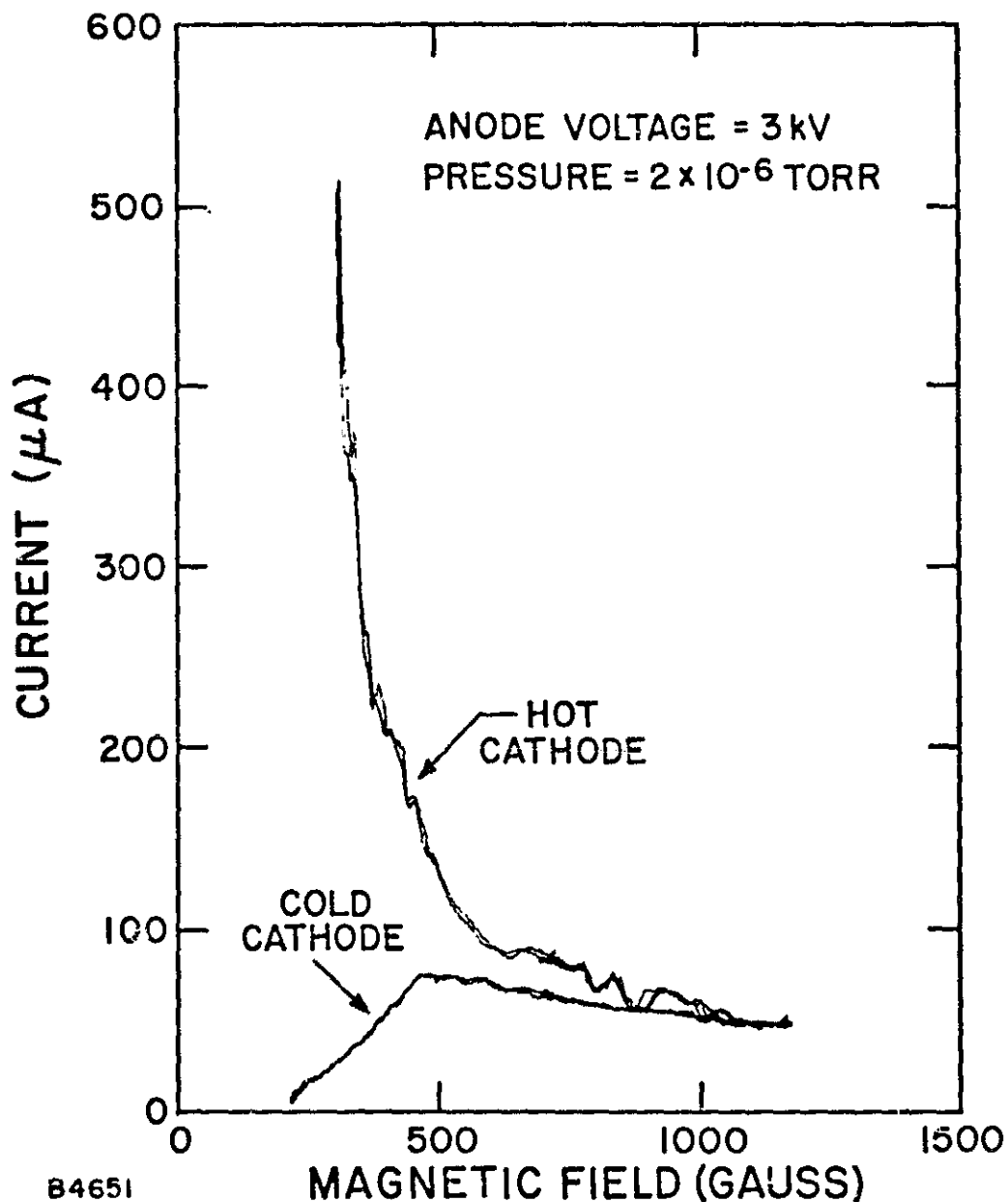


Fig. 4 Discharge current vs applied magnetic field (in the center of the coil) with conducting end-plates positioned 1 cm from the anode ( $z_e = 5.5$  cm). The two curves are for operation with hot and cold filament, respectively. Note the good reproducibility shown in the three overlays.



E1987

Fig. 5 Typical diocotron wave traces shown on a slow and a fast time scale.

### III. THEORY

The electrical characteristics of low-pressure ( $p < 10^{-4}$  Torr) Penning and magnetron discharges in a uniform magnetic field have been analyzed by several authors<sup>7-9</sup> and are now rather well understood. The occurrence of the diocotron instability at space charge saturation in these discharges has also been investigated and clarified.<sup>3, 12, 13</sup> Recent studies of a high-pressure ( $p > 10^{-4}$  Torr) Penning discharge in a strongly nonuniform mirror field<sup>14</sup> have demonstrated the existence of more complicated collective effects than are found at lower pressures and uniform magnetic fields.

First in this section, we use a simple one-dimensional model to derive characteristic discharge parameters. Secondly, we examine electron cloud equilibria in nonuniform magnetic fields and, finally, discuss possible sources of instability that could affect the containment in our experiment.

#### 1. Discharge Characteristics

Penning and magnetron discharges are maintained by electron impact ionization of the background neutral gas. The massive ions are not affected significantly by the magnetic field and, therefore, instantly move to the cathodes. This leads to build-up of a negative space charge cloud in the discharge volume; the electrons being confined radially by the magnetic field and axially by electrostatic forces. The space charge density of the electron cloud is determined by the balance of electron transport across the magnetic field and the rate of electron impact ionization of the background neutral gas. Since the rate of ionization is directly proportional to the background

pressure, the same proportionality applies to the current (pressure gauge). When the magnetic field is increased, the crossed-field mobility decreases, however, this increases the space charge density. The net result of this is an increase of the discharge current, as shown by the cold cathode curve in Fig. 4. At a certain value of the magnetic field (~ 450 G in the example of Fig. 4), the discharge becomes completely space charge limited.

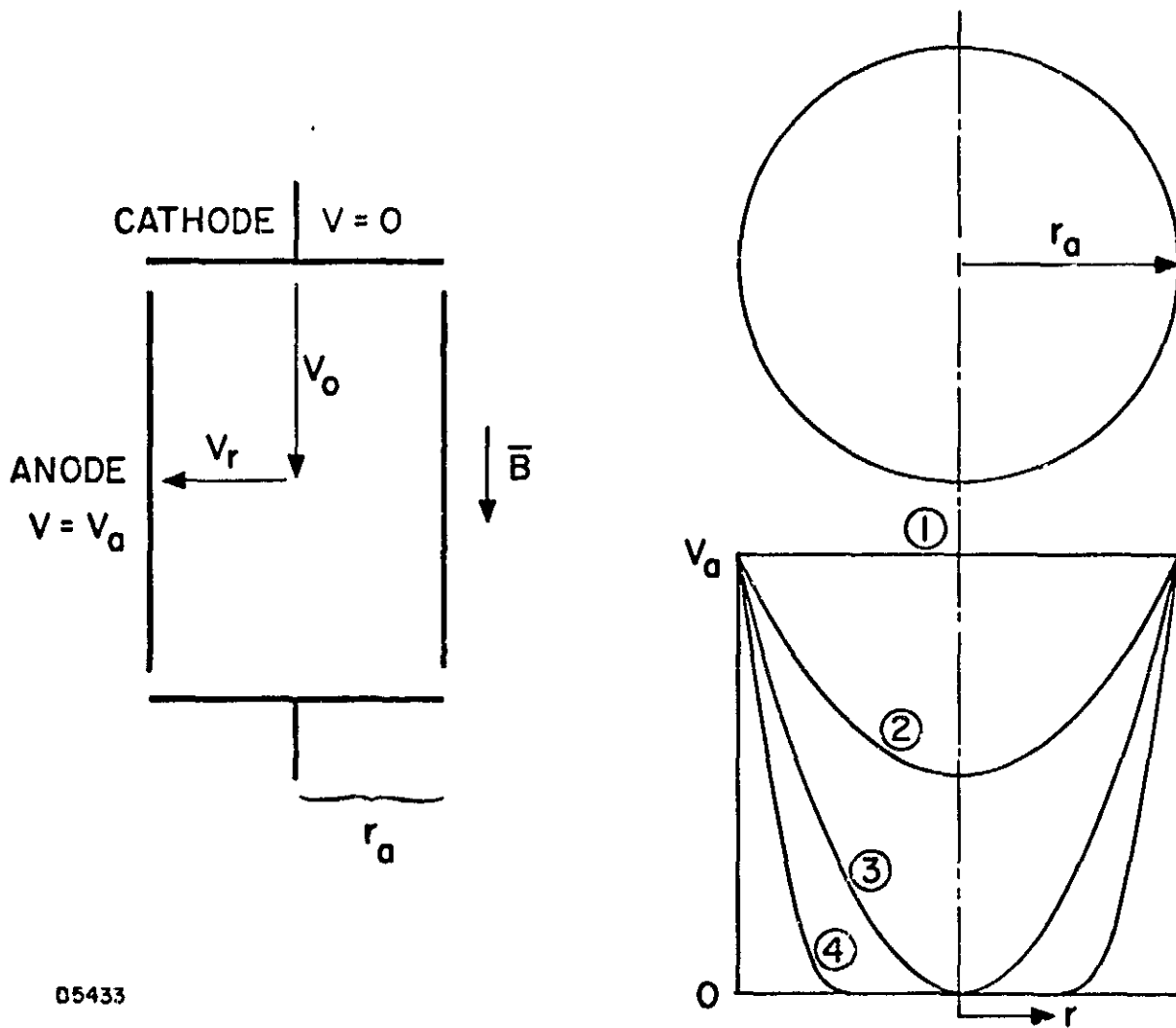
Although the vacuum electric field of the magnetron configuration is very different from that of the Penning configuration the discharge characteristics of the two devices are strikingly similar. The main reason for this similarity is the build-up of electron space charge. In the Penning discharge, the space charge creates a virtual cathode which converts the electric field from axial into radial, and in the limit of space charge saturation, the field shape of the two configurations is identical. To arrive at this limit, we consider the Penning geometry shown in Fig. 6. Here it is assumed that the anode voltage  $V_a$  can be divided into an axial component,  $V_o$ , and a radial component,  $V_r$ . The radial electric field follows from Poissons equation

$$\frac{1}{r} \frac{d}{dr} (rE_r) = - \frac{n_e e}{\epsilon_o} \quad (1)$$

The continuity equation for electrons can be written as

$$\frac{1}{r} \frac{d}{dr} (rn_e v_r) = n_e \nu_i \quad (2)$$

where  $\nu_i$  is the ionization frequency and  $v_r$  is the radial drift velocity of the electrons across the magnetic field B



05433

Fig. 6 a) Cylindrical Penning discharge geometry used as an idealized model for deriving discharge characteristics. b) Schematic representation of the radial potential profiles corresponding to different regimes of operation as explained in the text.

$$v_r = -\frac{4}{3} \frac{m}{e} v_{en} \frac{E_r}{B^2} \quad (3)$$

The quantity  $v_{en}$  is the total electron-neutral collision frequency. Assuming that  $v_i$  and  $v_{en}$  are constant the combination of Eqs. (1) - (3) gives for the electron density

$$n_e = \frac{3}{4} \frac{\epsilon_o B^2}{m} \frac{v_i}{v_{en}} \quad (4)$$

which is independent of  $r$ . Eq. (1) integrates to

$$E_r = \frac{en_e r}{2\epsilon_o} \quad (5)$$

This linear dependence of the electric field on the radius implies that the electron cloud rotates as a solid body with the frequency

$$f_l = \frac{en_e}{4\pi\epsilon_o B} \quad (6)$$

A second integration of Eq. (1) gives

$$V_a - V_o = \frac{en_e r_a^2}{4\epsilon_o} \quad (7)$$

where  $r_a$  is the radius of the anode. The total space charge of the electron cloud contained in a cylindrical anode of length  $L$  is therefore equal to

$$Q = \pi r_a^2 n_e L = (4\pi\epsilon_o) (V_a - V_o) L \quad (8)$$

It should be noted that  $Q$  is independent of the anode radius. Neglecting a small contribution due to secondary electrons, the cathode current can be expressed in terms of the volume ionization. Hence

$$I_c = Q v_i = (4\pi \epsilon_o)(V_a - V_o) L v_i \quad (9)$$

The electron current to the anode can be written as

$$I_a = 2\pi r_a n_e e v_a L \quad (10)$$

where  $v_a$  is the drift velocity  $v_r$  evaluated from  $r = r_a$ . Under steady state conditions,  $I_c = I_a$ .

We note that the discharge current as well as the electron density is expected to increase as  $B^2$ . This corresponds to the partially space-charge limited condition labeled (2) in Fig. 6. At a certain value of the magnetic field,  $B = B_s$ , the discharge becomes fully space charge limited,  $V_o = 0$  corresponding to curve (3) in Fig. 6, and the current reaches a saturation value

$$I_s = 4\pi \epsilon_o V_a L v_i \quad (11)$$

The magnetic field at the saturation point is

$$B_s^2 = \frac{16}{3} \frac{m}{e} \frac{v_{en}}{v_i} \frac{V_a}{r_a^2} \quad (12)$$

Equations (11) and (12) are also valid for the cylindrical magnetron configuration.

In our discussion we have assumed that any axial dependence of the electric field can be neglected. This assumption is justified in regions where electrons are present, for which we must have the condition  $\bar{E} \cdot \bar{B} = 0$  fulfilled. Near the cathode ends of the discharge, however, there is a region in which the electron density goes zero and the electric field

approaches the vacuum field determined by Laplace's equation. Consequently, the effective length of the confined electron cloud is always smaller than the length of the discharge cell. If the length of the cell is comparable to its diameter or smaller end effects will cause a considerable reduction of the discharge current given by Eq. (11).

## 2. Electron Cloud Equilibria

For a uniform magnetic field, the condition  $\bar{\mathbf{E}} \cdot \bar{\mathbf{B}} = 0$  is trivially fulfilled for  $n_e = \text{const.}$  along the magnetic field lines. The same condition applied to non-uniform, axially symmetric magnetic fields, such as the field shown in Fig. 3, has been considered by Levy.<sup>10</sup>

Following Levy, we can express the radial and axial components of the magnetic field as

$$B_r = -\frac{1}{r} \frac{\partial}{\partial z} (r A_\theta)$$

$$B_z = \frac{1}{r} \frac{\partial}{\partial r} (r A_\theta)$$
(13)

where the azimuthal component  $A_\theta$  of the magnetic vector potential is a function of  $r$  and  $z$ . Surfaces of constant magnetic flux are given by

$$\Phi = 2\pi r A_\theta = \text{const.}$$
(14)

The condition  $\bar{\mathbf{E}} \cdot \bar{\mathbf{B}} = 0$  is satisfied if the flux surfaces coincide with electrostatic equipotential surfaces, or

$$V(r, z) = F[\Phi(r, z)]$$
(15)

where  $F$  is an arbitrary function of  $\Phi$ . Taking the negative gradient of  $V$

and using Eq. (13) gives the two components of the electric field

$$\begin{aligned} E_r &= -2\pi r B_z \frac{\partial V}{\partial \Phi} \\ E_z &= 2\pi r B_r \frac{\partial V}{\partial \Phi} \end{aligned} \quad (16)$$

Poissons equation in two dimensions ( $r, z$ ) is

$$\frac{1}{r} \frac{\partial}{\partial r} (r E_r) + \frac{\partial}{\partial z} (E_z) = -\frac{n_e e}{\epsilon_0} \quad (17)$$

Insertion of Eq. (16) in Eq. (17) assuming  $\nabla \times \bar{B} = 0$ , yields

$$\frac{n_e e}{2\pi \epsilon_0} = r^2 B^2 \frac{\partial^2 V}{\partial \Phi^2} + 2B_z \frac{\partial V}{\partial \Phi} \quad (18)$$

which is a general expression for the equilibrium density distribution in an axisymmetric magnetic field.

Equation (18) is simplified considerably if we assume the boundary condition of uniform electron density,  $n_{e0}$ , as well as uniform magnetic field,  $B_0$ , in the plane of symmetry ( $z = 0$ ). These assumptions lead to

$$V(r, 0) = \frac{n_{e0} e r^2}{4 \epsilon_0} \quad (19)$$

$$\phi(r, 0) = \pi r^2 B_0 \quad (20)$$

Hence

$$V(r, z) = f_1 \cdot \phi(r, z) \quad (21)$$

where  $f_1$  is the rotation frequency of the electron cloud given by Eq. (6). Thus, provided that the discharge is completely space charge limited, the condition  $\vec{E} \cdot \vec{B} = 0$  implies solid-body rotation of the confined electron cloud with the frequency  $f_1 = V_a / \phi_a$ , where  $V_a$  is the anode voltage and  $\phi_a$  is the total magnetic flux inside the anode.

The electron density distribution given by Eq. (18) in this case is

$$n_e(r, z) = n_{e0} \frac{B_z(r, z)}{B_0} \quad (22)$$

### 3. Electron Cloud Stability

Three types of instabilities have been identified for magnetically confined electron clouds, namely (1) the magnetron instability,<sup>1</sup> (2) the diocotron instability<sup>2, 3</sup> and (3) the ion-electron resonance instability.<sup>4</sup>

The magnetron instability occurs for large values of the parameter  $q \equiv \omega_p^2 / \omega_c^2$  near one. The growth rate of this instability is  $\sim \frac{1}{2} q \omega_c e^{-2/q}$ . Taking the electron plasma frequency  $\omega_p = (n_e e^2 / \epsilon_0 m)^{1/2}$  and the electron gyro frequency  $\omega_c = eB/m$ , we can express  $q$  as

$$q = \frac{n_e m}{\epsilon_0 B^2} \quad (23)$$

Based on this equation, Eq. (4) can be rewritten as

$$q = \frac{3}{4} \frac{\nu_i}{\nu_{en}} \quad (24)$$

The ratio  $\nu_i / \nu_{en}$  is typically of the order 0.1, which then largely explains the good stability exhibited by low-pressure Penning and magnetron discharges below the space-charge saturation point (region 2 in Fig. 6).

When the magnetic field is increased beyond the value  $B_s$  given by Eq. (12) the uniform electron density model is no longer valid. In this high-field regime of operation (labeled 4 in Fig. 6), the electron cloud has been observed to contract into a space charge sheath near the anode, while a tenuous neutral plasma is formed on the axis of the discharge.<sup>13</sup> This electron cloud geometry is liable to become unstable due to the diocotron effect. The diocotron instability occurs for  $q \ll 1$  and its growth is attributed to the resonant coupling of electrostatic surface waves generated by density perturbations on two free surfaces of a magnetically confined electron cloud. According to theory, the  $\ell = 1$  mode in an infinite cylindrical geometry is always stable. The  $\ell = 2$  mode is the most unstable, in the sense that wave growth for this mode will occur for thicker charge layers than it will for higher modes. The diocotron wave frequency for azimuthal modes  $\ell$  is<sup>1</sup>

$$f_\ell = f_1 \left[ \ell - 1 + (r_c/r_a)^{2\ell} \right] \quad (25)$$

where  $f_1$  is the solid-body rotation frequency defined by Eq. (6) and  $r_c$ ,  $r_a$  are the radii of the cloud and the cylindrical wall, respectively. For  $r_c = r_a$  Eq. (25) reduces to  $f_\ell = \ell f_1$ .

The ion resonance instability, finally, requires that a certain fraction of ions are trapped within the electron cloud, and also that the characteristic frequency of ion oscillation in the electrostatic potential well is close to the frequencies of diocotron waves that can propagate on the surface of the electron cloud. This corresponds to having the ratio  $Zm_e/m_1q \sim 1$ . For singly ionized nitrogen,  $q$  would have to be of the

order of  $10^{-4}$  to satisfy this condition for instability. Although enhanced trapping of ions appears to occur beyond the space charge saturation point in Penning and magnetron discharges, the value of  $q \sim 0.1$  is much too high to explain the observed instability in this region in terms of ion resonance phenomena.

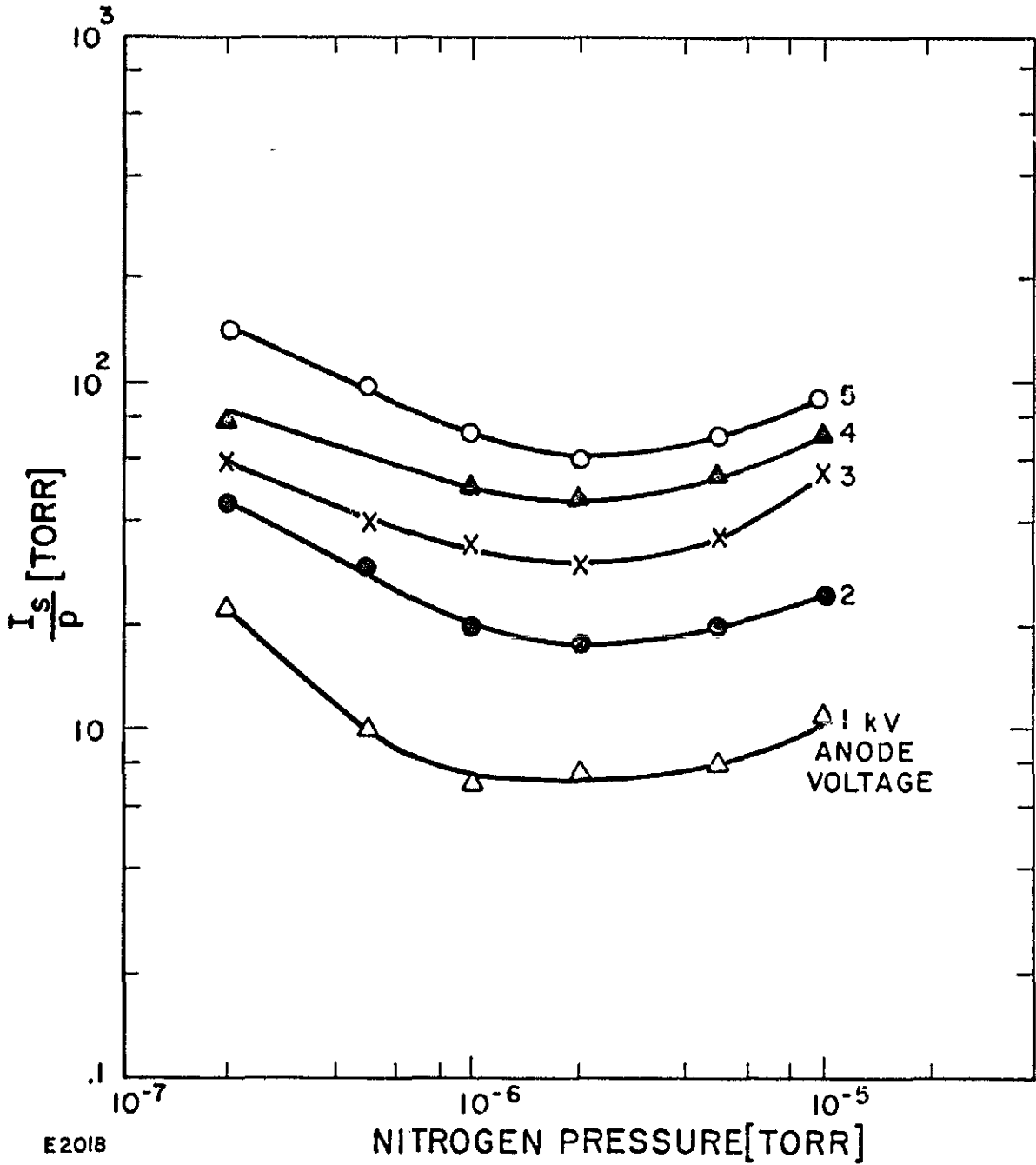
## IV. EXPERIMENTAL OBSERVATIONS

### 1. Discharge Current

The discharge current was measured as a function of the applied magnetic field for different gas pressures, anode voltages and end-plate positions. The symmetry of the discharge was checked by measuring the currents to the two end plates separately. Within the range of parameters investigated, the symmetry was found to be quite good, in that the current to one of the end plates never differed by more than 10% from the current to the other plate.

The option of running the filament hot was used only to a limited extent, primarily to confirm that space charge limited conditions were actually achieved. This is evidenced by the hot cathode curve shown in Fig. 4, in which case the emission limited current of the filament was several milliamperes. The steep drop in current before reaching the space charge limit is due to the Hull cutoff effect. Figure 4 also shows the excellent reproducibility obtained in the current measurements. The curves shown are composed of three overlays taken with increasing magnetic field.

The pressure dependence of the anode current is shown in Fig. 7 for the end plate location of  $z_e = 5.5$  cm (equivalent to 1 cm from the surface of the toroidal anode). The gas used throughout the experiments was nitrogen, and based on the results shown in Fig. 7, a standard pressure of  $2 \times 10^{-6}$  Torr was chosen for most of our studies in order to minimize uncertainties due to pressure variations.

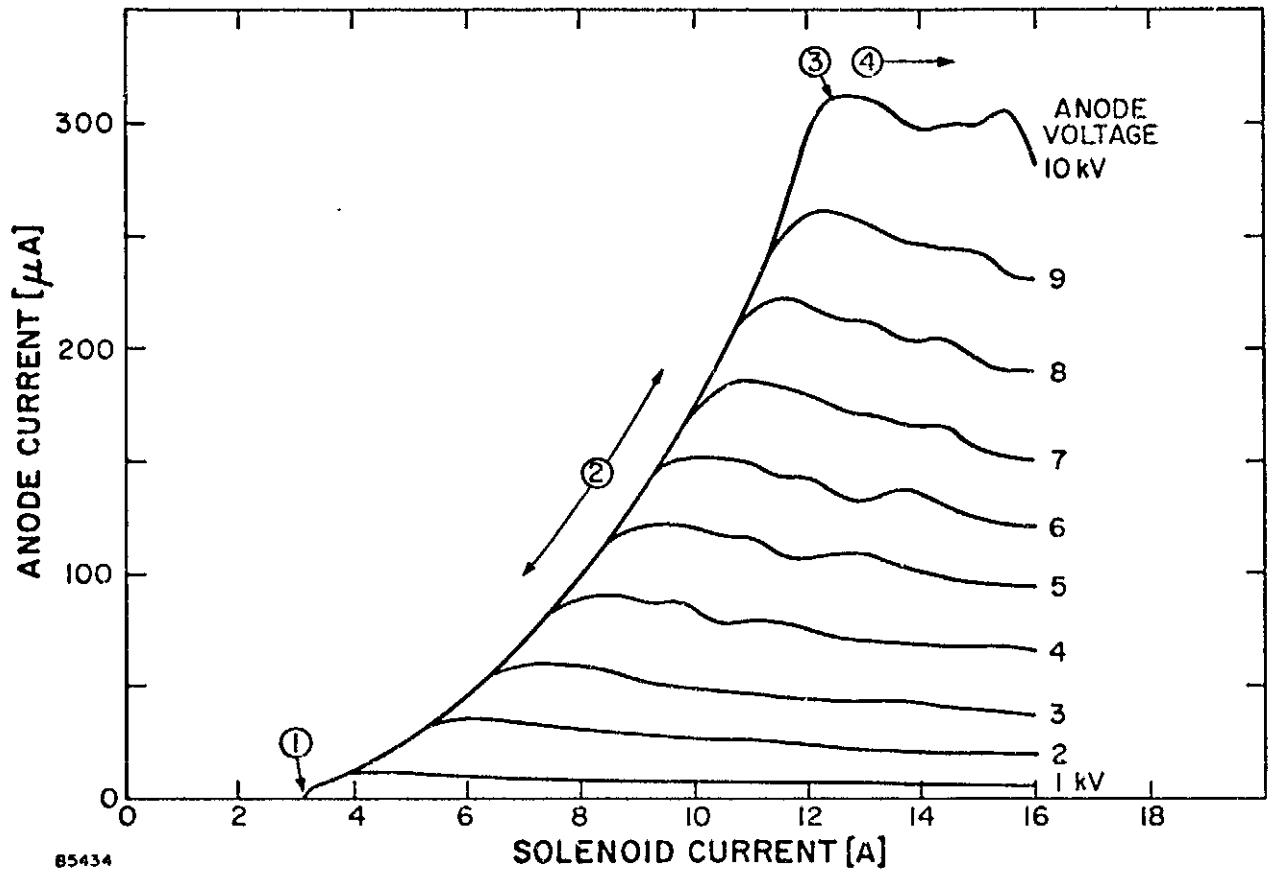


E2018

Fig. 7 Pressure and voltage dependence of the normalized discharge current for space charge saturated conditions. The minimum point at  $2 \times 10^{-6}$  Torr was selected for most of the experiments.

The discharge characteristics obtained for different anode voltages with  $z_e = 5.5$  cm are shown in Fig. 8. The overall behavior of the current is in agreement with the predictions of the simple model for the Penning discharge discussed in Section II-1. Along the rising portion of the curves, labeled (2), the current increases approximately proportional to  $B^2$ . The magnetic field  $B_s$  at the point of space charge saturation, labeled (3), has been plotted versus anode voltage in Fig. 9. The  $B_s \propto V_a^{1/2}$  dependence shown by this data is consistent with Eq. (12). Since the magnetic field strength and the radius of the anode both vary in  $z$ , we are not in a position, however, to directly evaluate the ratio  $\nu_i/\nu_{en}$ , as can be done for a one-dimensional discharge. The value of the saturation current  $I_s$  in Fig. 8 is shown as a function of  $V_a$  in Fig. 10. The dependence of  $I_s \propto V_a^{3/2}$  is the same as Schuurman<sup>9</sup> found for a cylindrical Penning discharge, and indicates that the ionization frequency  $\nu_i$  is proportional to the E/B velocity of the electrons (cf. Eq. (11)).

The next step in the experiments was to increase the distance between the end plates to allow the electron cloud to occupy regions of lower magnetic field. In this process, discharge characteristics were recorded for plate distances  $z_e$  up to 14.5 cm. A general observation was that the saturation point for a given anode voltage was displaced toward higher magnetic fields when the plate spacing was increased. The discharge current also kept increasing when  $z_e$  was increased. These features are evident in Fig. 11, which shows the discharge characteristics obtained for  $z_e = 14.5$  cm. The saturation currents measured for values of  $z_e$  between 4.5 cm and 14.5 cm are shown in Fig. 12.



85434

Fig. 8 Discharge characteristics obtained for  $p = 2 \times 10^{-6}$  Torr with the end-plates positioned at  $z_e = 5.5$  cm. The curves show the discharge current as a function of the magnetizing current in the solenoid ( $I_M = 1$  A gives 70 Gauss in the center of the coil) for several anode voltages. Different regimes of operation are indicated (cf. Fig. 6):

- (1) Cut-off point, below which the electron energy is too low to produce ionization.
- (2) Partially space charge limited region. Stable operation with the current governed by classical crossed-field mobility.
- (3) Space charge saturation point, appearance of diocotron waves.
- (4) High magnetic field region. Unstable due to contraction of the electron cloud.

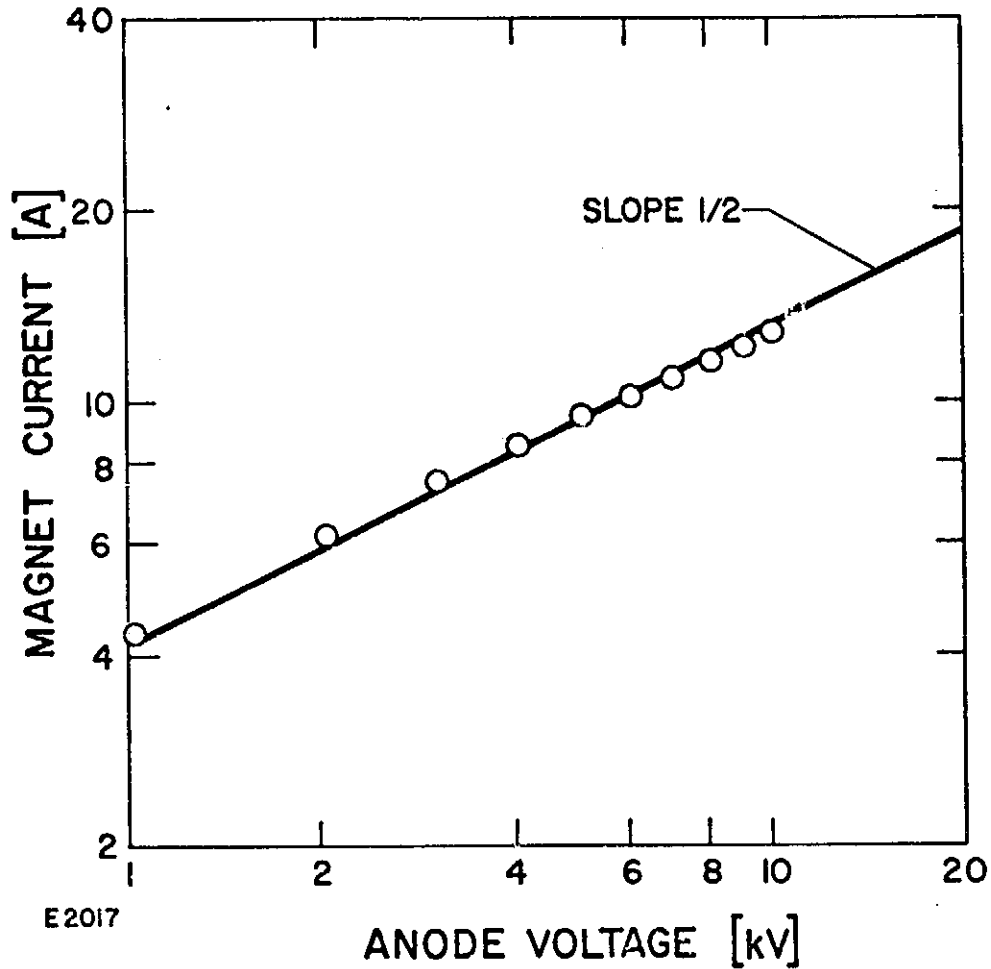
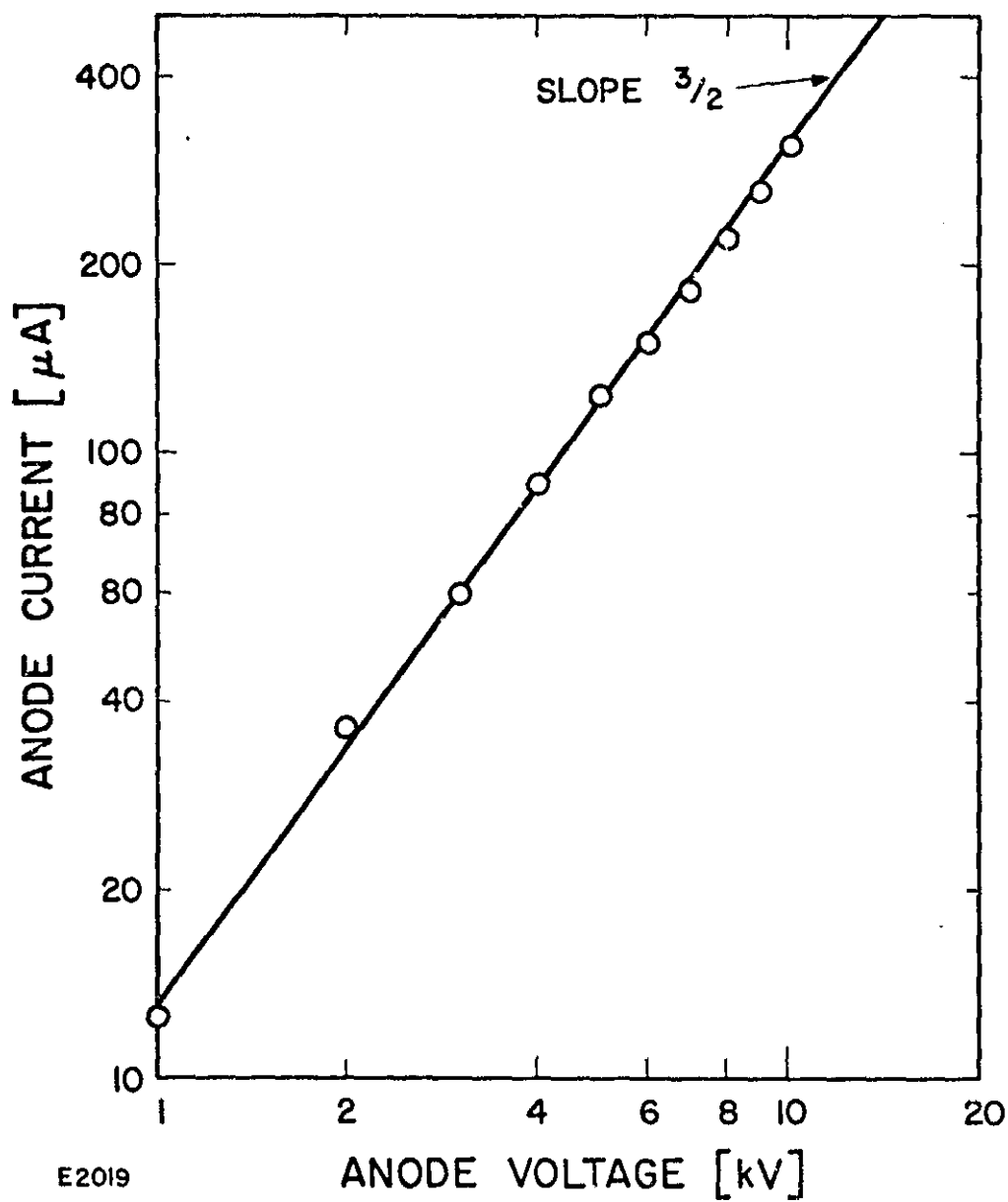


Fig. 9 Relationship between anode voltage  $V_a$  and magnetic field  $B_s$  (in terms of  $I_m$ ) at the space charge saturation point (3) for the data shown in Fig. 8. The  $B_s \propto V_a^{1/2}$  dependence is discussed in the text.



E2019

Fig. 10 Discharge current  $I_s$  at the saturation point (3) for the data shown in Fig. 8. The  $I_s \propto V_a^{3/2}$  dependence is discussed in the text.

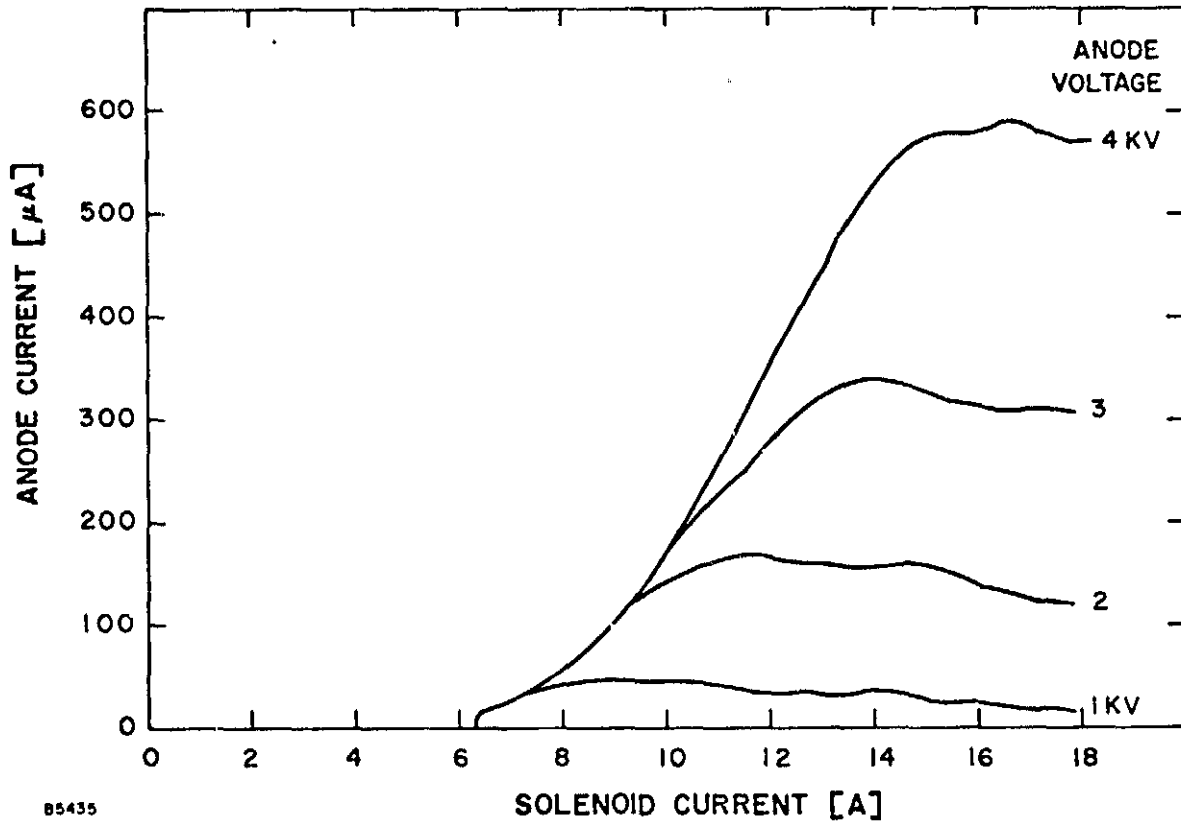


Fig. 11 Discharge characteristics obtained for  $p = 2 \times 10^{-6}$  Torr with end-plates positioned far apart ( $z_e = 14.5$  cm).

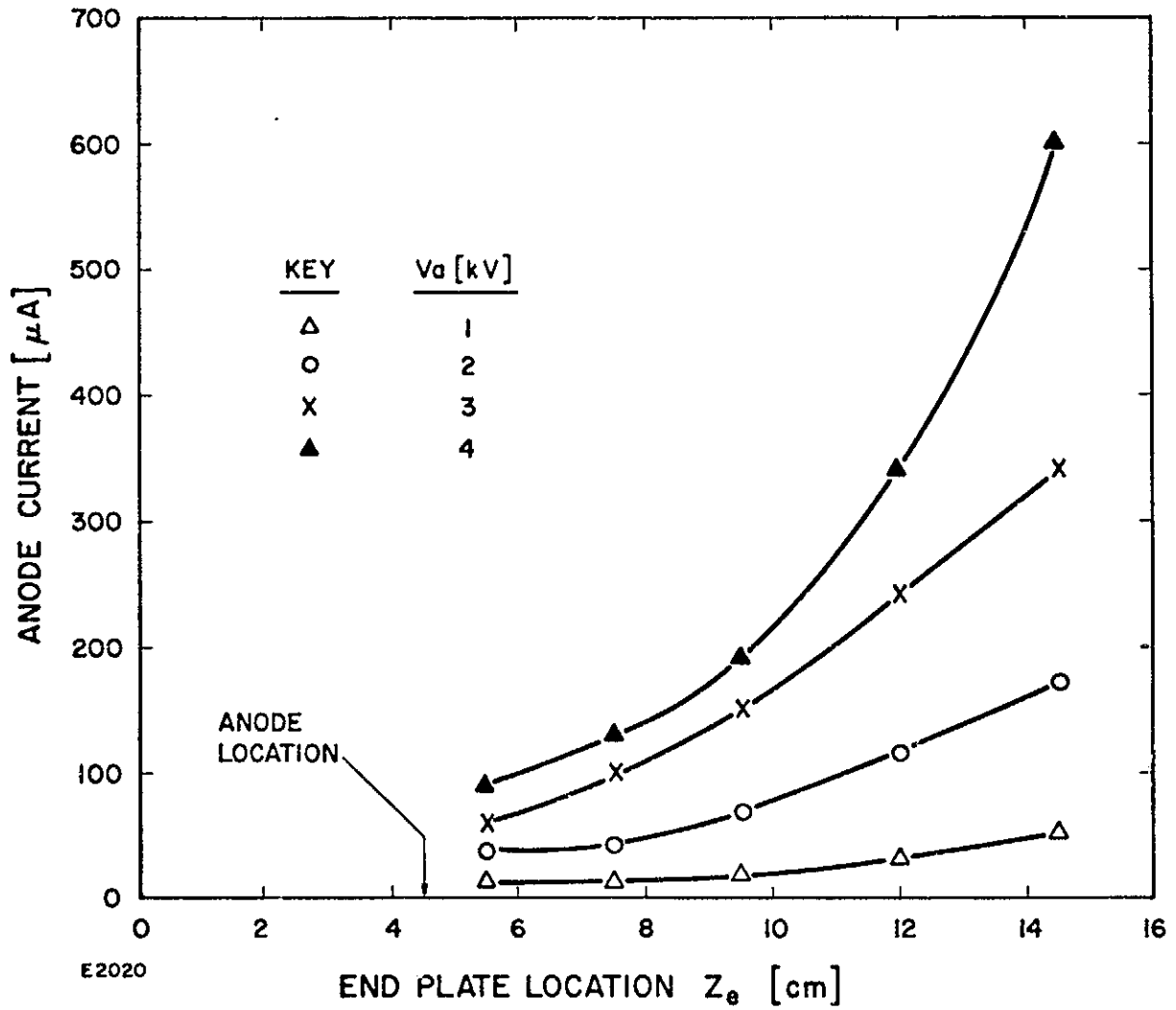
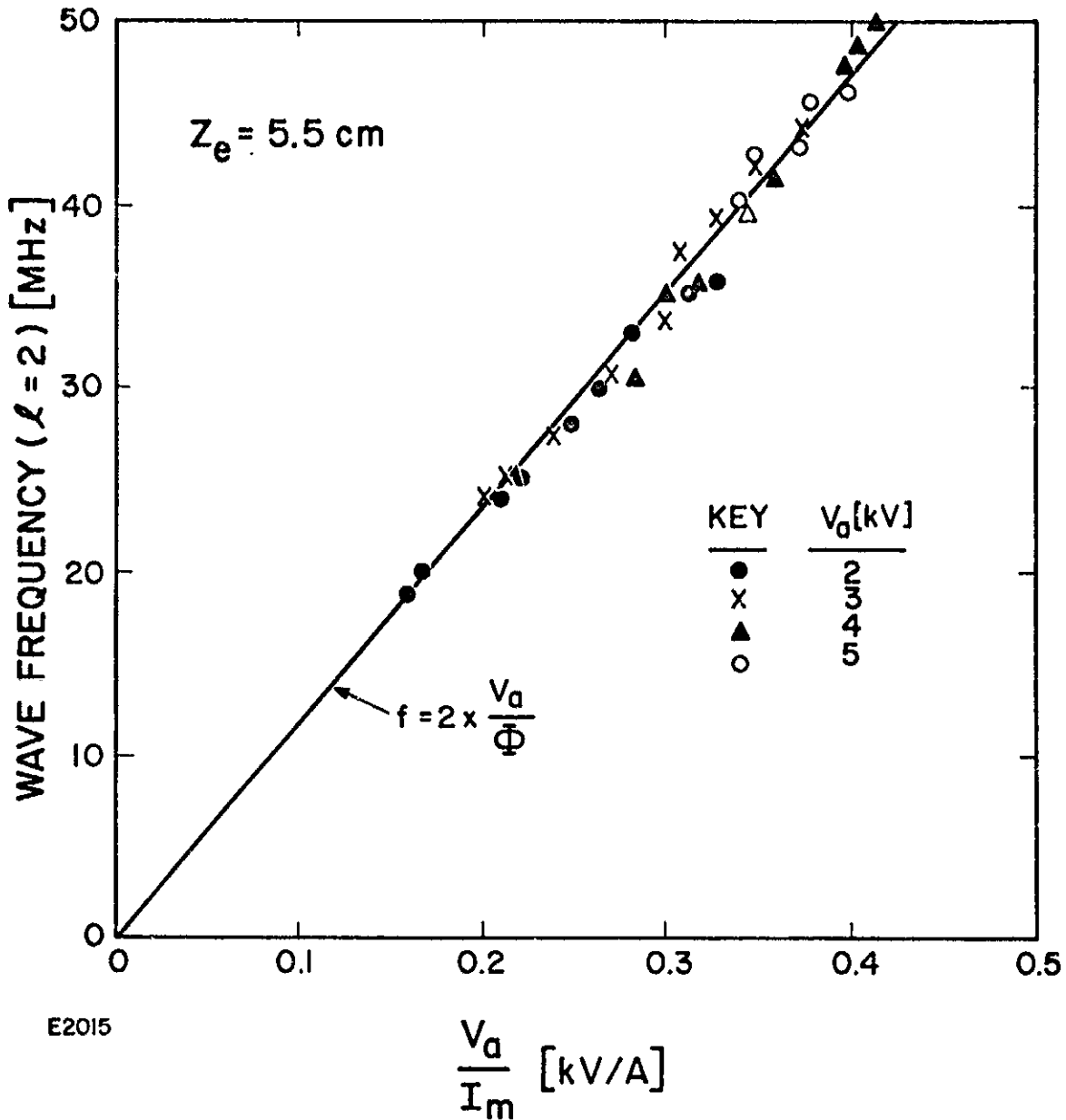


Fig. 12 Saturation current  $I_s$  at as a function of end-plate location for different anode voltages.

## 2. Diocotron Waves

The onset of diocotron waves, as measured with the current-buttons located on the end-plates, was always found to occur close to the space-charge saturation point ( $I_s, B_s$ ). For lower values of  $B < B_s$  the discharge was quiescent. The dominant diocotron wave mode observed was the  $\ell = 2$  mode, as identified from phase measurements using several current-buttons at different azimuths. The  $\ell = 1$  mode, predicted to be stable in an infinite cylinder,<sup>2</sup> was found to exist in the present configuration. For  $B > B_s$  the amplitude of the waves increased and so did the content of higher harmonics. Figure 5 shows typical oscilloscope traces of current-button signals on a slow time scale (upper trace) as well as on a fast time scale (lower trace). The period of the growth and decay shown by the upper trace was found to be approximately inversely proportional to the background gas pressure, which demonstrates that the instability is controlled by the build-up of space charge through ionization. Most of the frequency measurements were performed using a spectrum analyzer. The  $\ell = 2$  mode frequencies measured with the end plates located at  $z_e = 5.5$  cm are shown in Fig. 13, plotted as a function of the ratio of anode voltage to magnet current. The straight line drawn in this figure corresponds to twice the frequency for solid-body rotation, i.e.,  $f = 2f_1 = 2V_a/\phi_a$ .

Figure 14 shows frequency spectra obtained with the end plates moved further away from the anode ( $z_e = 12$  cm). The frequencies corresponding to the fundamental mode as well as  $\ell = 2$  and  $\ell = 3$  are closely grouped and within 10% of the calculated value  $f = \ell \times V_a/\phi_a$ .



E2015

Fig. 13 The points show measured  $\ell = 2$  mode diocotron wave frequencies plotted vs the ratio of anode voltage to magnet current. In this case the end-plates were located close to the anode ( $z_e = 5.5 \text{ cm}$ ). The theoretical line is for solid body rotation of a space charge saturated electron cloud.

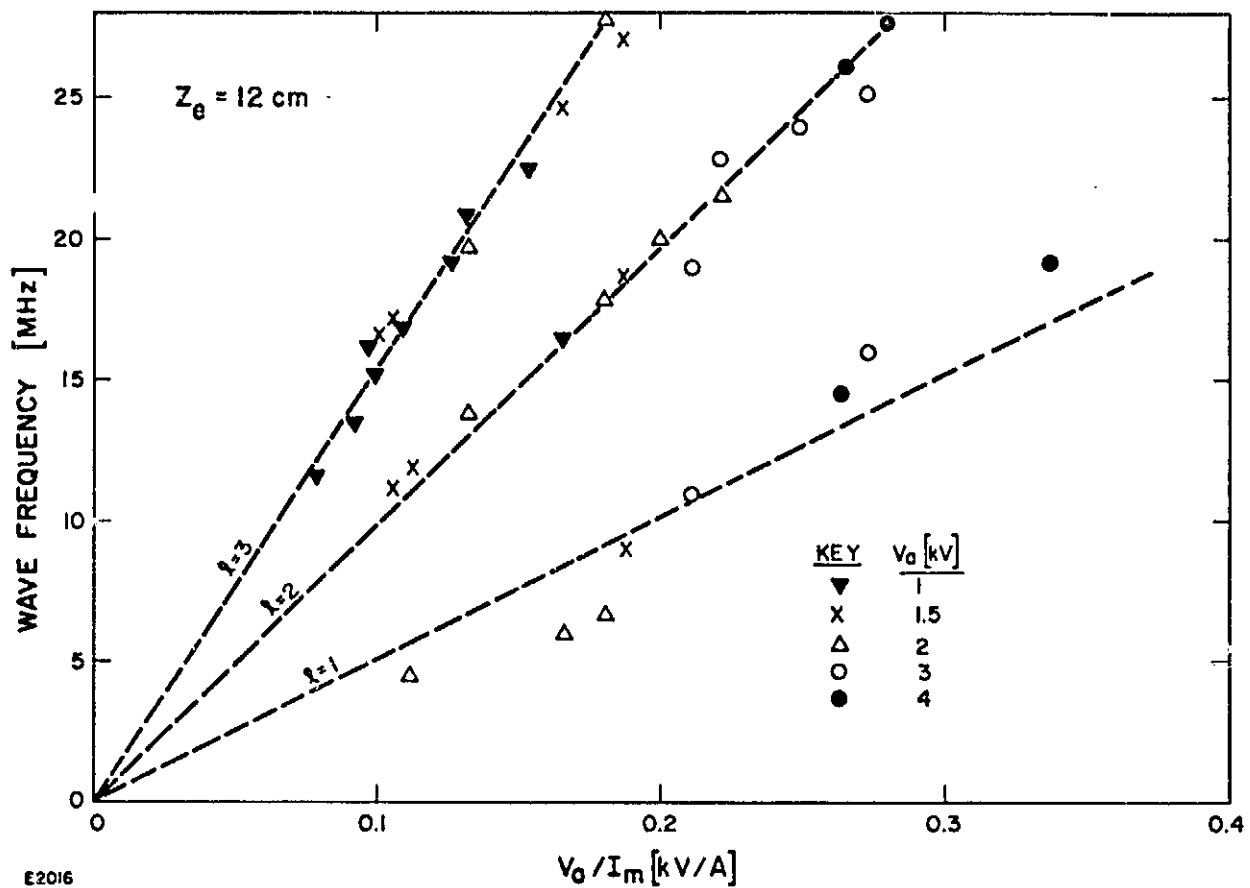
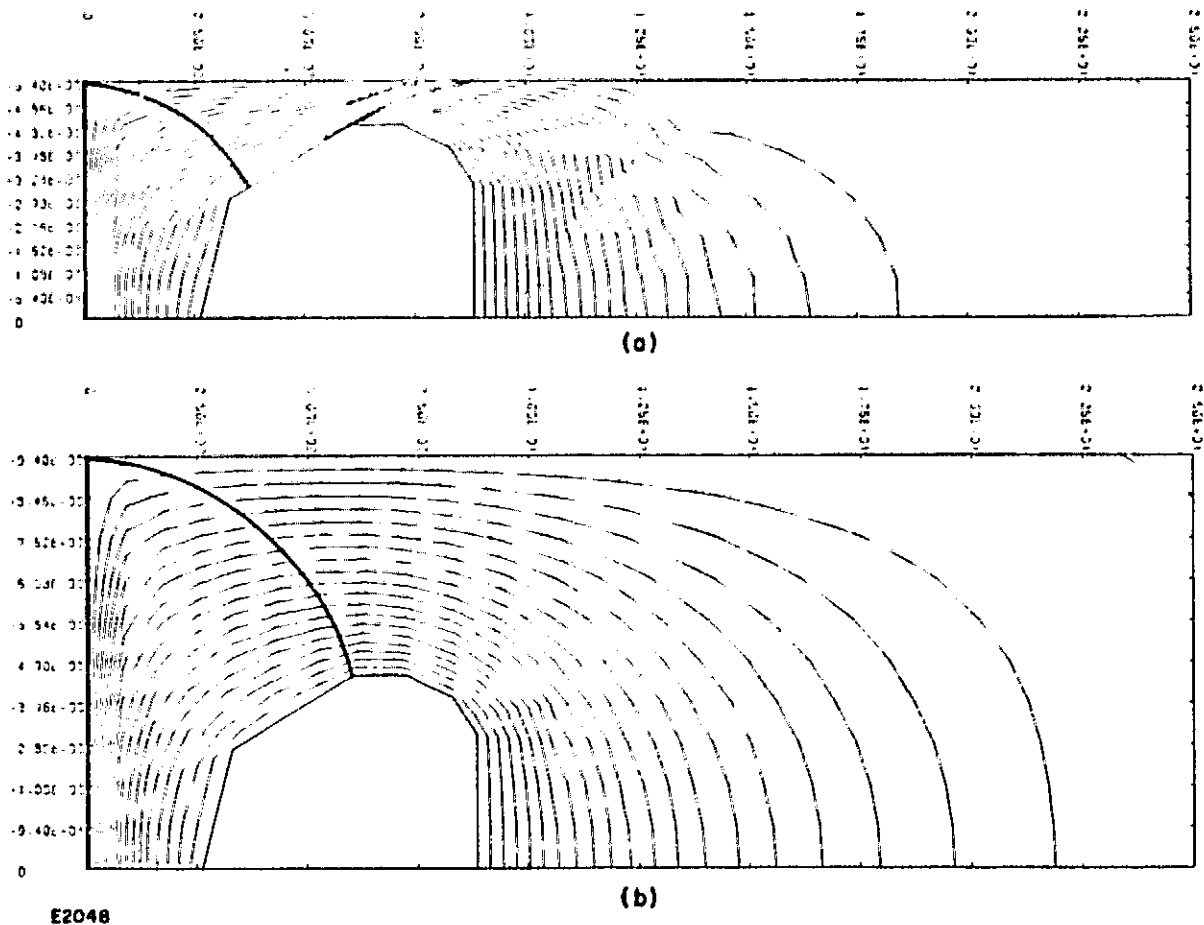


Fig. 14 Diocotron wave frequency spectrum measured with the end plates located far apart ( $z_e = 12 \text{ cm}$ ). The frequencies for the distinct modes observed are all close to the value associated with solid-body rotation.

## V. DISCUSSION AND CONCLUSIONS

The frequency measurements strongly suggest that the electron cloud in the space charge saturated discharge rotates as a solid body. Based on this condition, we can infer a spatial electron density distribution in accordance with Eq. (22), which simply says that  $n_e$  is proportional to the z-component of the magnetic field,  $B_z$ . Since  $B_z$  decreases rapidly as a function of the distance from the point of symmetry (cf. Fig. 3), one would expect a concentration of electrons in the central part of the coil-anode structure. The curvature of the magnetic field lines implies that  $B_z$  changes sign at some distance from the coil. This leads to the unphysical condition of negative electron densities which, however, arises from the fact that we have not yet applied the proper boundary condition given by the presence of the negative end-plates. On both sides of the free boundary where the electron density goes to zero we must have  $\vec{E} \cdot \vec{B} = 0$ , which implies that the equipotential lines must break away smoothly from the magnetic field lines without changing slope at the boundary. Since no straightforward method exists to calculate the exact boundary of the electron cloud in the present geometry,<sup>10</sup> we have attempted to find an upper limit on the volume occupied by electrons by matching the electrostatic potential inside the electron cloud given by Eq. (21) to the vacuum potential given by the solution of Laplace's equation. This approximation is quite crude when the end-plates are located close to the plane of symmetry, but should give more accurate results for larger  $z_e$ . Figure 15 shows the boundary of the



E2048

Fig. 15 Computer solutions of Laplace's equation for two different end-plate locations (a)  $z_e = 5.4$  cm and (b)  $z_e = 9.4$  cm. Equipotentials shown are spaced 5% apart. Matching of these equipotentials to the lines of constant flux shown in Fig. 3 gives the estimate of the electron cloud boundary indicated by the heavy lines.

REPRODUCIBILITY OF THE ORIGINAL PAGE IS POOR

electron cloud estimated by this method for two different values of  $z_e$ . In order to estimate the discharge current produced by volume ionization (cf. Eq. 11 for a one-dimensional discharge), this boundary was used for numerical evaluation of the integral

$$I_s = \iint n_e(r, z) e v_i(r, z) 2\pi r dr dz \quad (26)$$

where  $n_e(r, z)$  is given by Eq. (22) and the ionization frequency  $\nu_i(r, z)$  is assumed to be a function of the local crossed-field drift velocity  $E/B$ . The function  $\nu_i = f(E/B)$  for nitrogen was obtained from Ref. 9. The currents predicted by Eq. (26) for different end-plate distances and anode voltages are shown in Fig. 16 together with the measured currents (same as in Fig. 12).

The good agreement between measured and calculated currents for large values of  $z_e$  shown in Fig. 16 indicates that the assumed electron density distribution must be correct. The systematically increasing deviation of the computed current from the measured current when  $z_e$  is decreased is attributed to the less accurate estimate of the electron cloud boundary for small  $z_e$ .

Regarding the stability of the electron cloud, we note that although the electron density decreases as  $B_z$ , the value of  $q$  is proportional to  $B_z/B^2$  and, therefore,  $q$  will increase with distance going from higher to lower magnetic field regions. Thus, for a large distance between the end-plates,  $q$  could become close to one near the free boundary of the electron cloud. Since the discharge was found to be quiescent up to the space charge saturation point even for large  $z_e$ , there is no evidence in

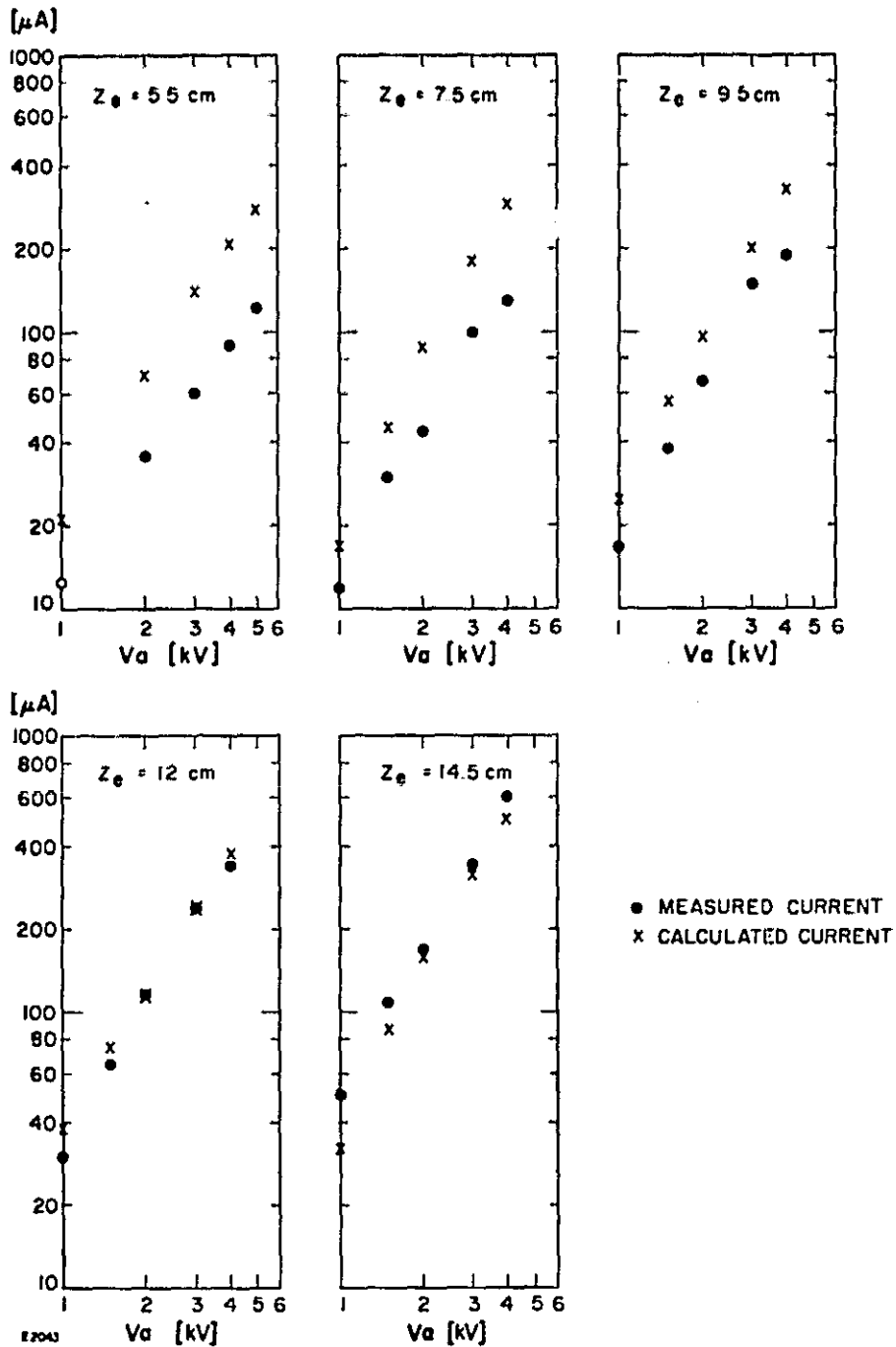


Fig. 16 Comparison of measured and calculated currents for different end-plate locations. The calculated values are based on total ionization within the volume enclosed by the anode and the boundary shown in Fig. 15.

the present experiments that a high value of  $q$  in low density regions would affect the overall stability of the electron cloud.

In summary, experiments were performed with a low-pressure, crossed-field discharge utilizing a nonuniform, axisymmetric magnetic field. Measurements of discharge current and diocotron wave frequency show that the electron cloud formed in the discharge is concentrated to the region of high magnetic field and, under space charge saturated conditions, rotates as a solid body. These observations are consistent with the condition that in regions occupied by electrons the magnetic field lines are electrostatic equipotentials.

## VI. ACKNOWLEDGMENTS

It is a pleasure to acknowledge useful discussions with J. D. Daugherty, G. S. Janes, R. H. Levy, and J. Jacob. The technical assistance of J. Dotson and D. Twombly is highly appreciated.

PRECEDING PAGE BLANK NOT FILMED

## VII. REFERENCES

1. O. Buneman, R. H. Levy, L. M. Linson, J. Appl. Phys. 37, 3203 (1966).
2. R. H. Levy, Phys. Fluids 8, 1288 (1965).
3. W. Knauer, J. Appl. Phys. 37, 602 (1966).
4. R. H. Levy, J. D. Daugherty, O. Buneman, Phys. Fluids 12, 2616 (1969).
5. J. D. Daugherty, J. E. Eninger, G. S. Janes, Phys. Fluids 12, 2677 (1969).
6. J. D. Daugherty, R. H. Levy, Phys. Fluids 10, 155 (1967).
7. J. C. Helmer, R. L. Jepsen, Proc. of the IRE 49, 1920 (1961).
8. R. L. Jepsen, J. Appl. Phys. 32, 2619 (1961).
9. W. Schuurman, "Investigation of a Low-Pressure Penning Discharge," FOM-Instituut voor Plasma-Fysica, Rijnhuizen Report 66-28.
10. R. H. Levy, Phys. Fluids 11, 772 (1968).
11. R. H. Levy, G. S. Janes, AIAA J. 2, 1835 (1964).
12. W. Knauer, A. Fafarman, R. L. Poeschel, Appl. Phys. Letters 3, 111 (1963).
13. W. Knaue R. L. Poeschel, Proceedings of the 7th International Conference on Phenomena in Ionized Gases, Belgrade, Vol. II, 719 (1965).
14. N. Hopfgarten, R. B. Johansson, B. H. Nilsson, H. Persson, "Collective Phenomena in a Penning Discharge in a Strongly Inhomogeneous Magnetic Field," TRITA-EPP-72-13, Dept. Electron and Plasma Physics, Royal Inst. Technology.

PRECEDING PAGE BLANK NOT FILLED

## DOCUMENT CONTROL DATA - R &amp; D

(Security classification of title, body of abstract and indexing annotation not to be entered when the overall report is classified)

1 ORIGINATING ACTIVITY (Corporate author) AVCO EVERETT RESEARCH LABORATORY, INC. 2385 REVERE BEACH PARKWAY EVERETT, MASSACHUSETTS 02149		2a. REPORT SECURITY CLASSIFICATION Unclassified	
3 REPORT TITLE EXPERIMENTAL INVESTIGATION OF ELECTRON CLOUD CONTAINMENT IN A NONUNIFORM MAGNETIC FIELD		2b. GROUP	
4 DESCRIPTIVE NOTES (Type of report and inclusive dates) Research Report 400			
5 AUTHOR(S) (First name, middle initial, last name) J. E. Eninger			
6 REPORT DATE May 1974	7a. TOTAL NO OF PAGES 41	7b. NO OF REFS 14	
8a. CONTRACT OR GRANT NO NAS8-24140	8b. ORIGINATOR'S REPORT NUMBER(S) Research Report 400		
b. PROJECT NO	8c. OTHER REPORT NO(S) (Any other numbers that may be assigned this report)		
c.			
d.			
10 DISTRIBUTION STATEMENT			
11 SUPPLEMENTARY NOTES		12 SPONSORING MILITARY ACTIVITY George C. Marshall Space Flight Center, NASA, Marshall Space Flight Center, Alabama 35812	
13 ABSTRACT Dense clouds of electrons are generated and studied in an axisymmetric, nonuniform magnetic field created by a short solenoid. The operation of the experiment is similar to that of a low-pressure ( $\sim 10^{-6}$ Torr) magnetron discharge. Discharge current characteristics are presented as a function of pressure, magnetic field strength, voltage, and cathode end-plate location. The rotation of the electron cloud is determined from the frequency of diocotron waves. In the space charge saturated regime of operation, the cloud is found to rotate as a solid body with a frequency close to $V_a/\phi_a$ where $V_a$ is the anode voltage and $\phi_a$ is the total magnetic flux. This result indicates that, in regions where electrons are present, the magnetic field lines are electrostatic equipotentials ( $\vec{E} \cdot \vec{B} = 0$ ). Equilibrium electron density distributions suggested by this condition are integrated with respect to total ionizing power and are found consistent with measured discharge currents.			

14 KEY WORDS	LINE A		LINE B		LINE C	
	ROLL	WT	ROLL	WT	ROLL	WT
1. Crossed-Field Devices 2. Magnetron Discharge 3. Electron Plasma 4. Electron Cloud Equilibrium 5. Electron Cloud Stability						